

# Systematic Design Technique for Dual-Band Branch-Line Coupler Using T- and Pi-Networks and Their Application in Novel Wideband-Ratio Crossover

Mohammad A. Maktoomi, *Graduate Student Member, IEEE*, Mohammad S. Hashmi, *Member, IEEE*, and Fadhel M. Ghannouchi, *Fellow, IEEE*

**Abstract**—In this paper, a generalized analysis and design methodology of a dual-band branch-line coupler (BLC) is presented. The proposed design, although based on the prevalent method of replacement of various arms of a single-band BLC with an equivalent T-/Pi-network, simplifies the design approach by only replacing either pair of arms and therefore provides four distinct topologies. Closed-form design equations along with insightful comments are reported for all the four topologies of the BLC. A number of cases are investigated to demonstrate the effectiveness of the proposed design for equal and unequal power division ratio and band-ratio ( $=f_2/f_1$ ). As an application, a novel dual-band crossover as a cascade of BLCs is also presented. While investigating the limitations of previous designs, a strategy to obtain the crossover with so far the widest band-ratio and simple layout is also presented. An unequal power division dual-band BLC and a dual-band crossover are designed which operate at 1/2 and 1/4 GHz, respectively. These designs are validated from the electromagnetic simulations and prototypes implemented on RT/Duroid 5880 substrate.

**Index Terms**—Coupler, crossover, dual band, microstrip, multiband, unequal power division.

## I. INTRODUCTION

A BRANCH-LINE coupler (BLC) is a four-port high-frequency device that is frequently used for power combining/splitting. For example, they are widely used in balanced amplifiers, mixers, beam-forming networks, and antenna arrays [1], [2]. On the other hand, a crossover is also a four-port matched device similar to a BLC. As is implied by its name, two signal paths are allowed to cross each other, ideally with infinite isolation by a crossover. A crossover can also be interpreted as a 0-dB coupler and is used in applications such as Butler matrix for antenna arrays [3].

Manuscript received August 25, 2015; revised January 5, 2016 and March 4, 2016; accepted March 15, 2016. Date of publication April 21, 2016; date of current version May 13, 2016. Recommended for publication by Associate Editor T.-L. Wu upon evaluation of reviewers' comments.

M. A. Maktoomi and M. S. Hashmi are with Circuit Design Research Lab, Indraprastha Institute of Information Technology Delhi, New Delhi 110020, India, and also with the iRadio Laboratory, University of Calgary, Calgary, AB T2N 1N4, Canada (e-mail: ayatullahm@iiitd.ac.in; mshashmi@iiitd.ac.in).

F. M. Ghannouchi is with the iRadio Laboratory, University of Calgary, Calgary, AB T2N 1N4, Canada (e-mail: fghannou@ucalgary.ca).

Color versions of one or more of the figures in this paper are available online at <http://ieeexplore.ieee.org>.

Digital Object Identifier 10.1109/TCPMT.2016.2548498

In recent years, dual-band/multiband and reconfigurable components have been given a lot of attention due to their potential use in cognitive/software-defined radios [4]–[14]. This has led to development of numerous dual-band BLCs and crossovers [15]–[37].

The most common approach to design a dual-band BLC is by the simple replacement of all the quarter-wave lines of a single-band BLC with equivalent dual-band quarter-wave blocks. The composite right-/left-hand transmission lines (TLs) [15], Pi-network [16], [17], T-network [18], recently reported modified T-network incorporating coupled line [19], and stepped impedance with open/short stub lines [20], [21] are a few examples of dual-band quarter-wave blocks. These reported designs have either limited band-ratio or complex design procedure or they provide a means of obtaining only equal power division. A few modifications to the Pi-network-based dual-band BLCs have also been reported, for instance, in [22] to obtain tunability around the two frequencies, in [23] to generalize the same, and, recently, in [24] to achieve arbitrary phase along with arbitrary power division.

Another technique is to show a particular structure to be a dual-band BLC; in this context, a coupled line-based BLC was proposed in [25], and further improvements were reported to get unequal power division [26], [27]. Similar approach was also adopted in the design of a cross line coupler [28]. Examples making uses of coupled line are difficult to tune for good performance at two frequencies due to inherent unequal even/odd-mode velocities in microstrip technology [25], while a larger area is required for the realization of a dual-band coupler reported in [28].

More recently, some of the dual-band coupler design techniques [13], [29] that are based on the impedance matching concept employ the dual-band equivalent of the port extension techniques [30], [31]. However, larger board size is often required in this technique, especially when cascading, for example, to achieve a wider bandwidth.

The dual-band crossover reported in [34] is a three-section branch-line structure which needs larger area whereas the crossover design reported in [35] has complex layout. In fact, a modified version of window-shaped structure using

a T-network [35] has been reported very recently which uses an asymmetric Pi-network to get improved band-ratio [38]. However, the board layout is too complex owing to the presence of eight stubs inside the window. Moreover, if the stub length is taken as an integer multiple (for example, = 2) of the usual length, as is sometimes required [14], then the same cannot even be fabricated. A dual-band crossover as cascade of two dual-band couplers reported in [36] and a simplified two-section crossover [37] have limited band-ratio.

Traditionally, when a dual-band BLC is obtained by incorporating a T-/Pi-network, it is the single-band BLC of *equal length* which is at the core and thus, replacement of all the four arms is required in this procedure [14]. An interesting and the first successful conversion of a single-band BLC of unequal branch lengths into a dual-band BLC using a T-network was presented in [32]. However, it is limited for equal power division only. Furthermore, the paper does not provide any logical discussion regarding replacement of only one of coupler's arm pair by a T-network which essentially leads to problem in analyzing and estimating the performance metrics of this design.

In this paper, a simplified systematic approach, which is more generalized, to design a dual-band BLC and crossover with unequal branch lengths is proposed. The key contributions of this paper are as follows.

- 1) A generalized theory of conversion of an unequal length single-band coupler into a dual-band coupler utilizing T-networks is reported with clear mathematical analysis which is also duly backed by intuitive reasonings.
- 2) The developed generalized theory for an unequal length dual-band coupler using a T-network has been for the first time extended to an unequal length dual-band coupler using Pi-networks. In this process, it is also demonstrated that it is advantageous to use a T-network for higher band-ratios whereas a Pi-network performs better for lower band-ratios. In addition, it is also shown that two dual-band coupler topologies, but equivalent structures, are possible with a Pi-network.
- 3) Finally, strategy to design dual-band crossover using a T-type network, with very high band-ratio is proposed. In fact, by providing proper interpretation, correction and modification of a previously reported crossover [36] along with the proposed crossover structure, a strategy to come up with a crossover having the widest band-ratio so far and simple layout is presented.

Remainder of this paper consists of the review of a single-band unequal length BLC in Section II, an elaborated discussion on possible structures of the proposed couplers in Section III, and the implementation strategy of the proposed dual-band crossover in Section IV. Section V provides discussion on simulated results. For demonstration purposes, prototypes developed along with the measurement results are presented in Section VI, whereas Section VII presents a few concluding remarks.

## II. REVIEW OF UNEQUAL LINE LENGTH COUPLER

An unequal length BLC is shown in Fig. 1, which has, for example,  $Z_a$  and  $\theta_a$  as the characteristic impedance and

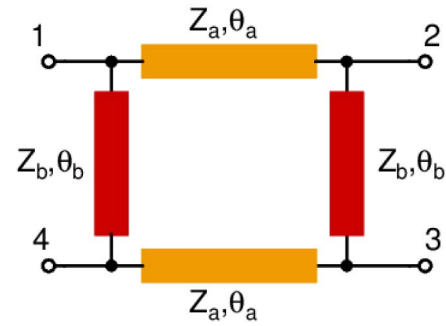


Fig. 1. Single-band unequal length BLC.

electrical length of the horizontal TL sections, respectively. The corresponding terms for the vertical TL sections are  $Z_b$  and  $\theta_b$ . Port 1 is the input port whereas Ports 2 and 3 are the through and coupled ports, respectively, and Port 4 is the isolated port. The power division ratio,  $\alpha$  ( $0 < \alpha^2 < 1$ ), is defined such that

$$P_2 = \alpha^2 P_1 \quad (1)$$

where  $P_2$  = power output through Port 2 and  $P_1$  = power input to Port 1.

The conditions that the structure of Fig. 1 behaves as a single-band BLC were discussed in [39]. In this context, the parameters of the BLC can be expressed as

$$Z_a = \frac{\alpha Z_0}{\sqrt{\alpha^2 + (1 - \alpha^2) \sin^2 \theta_b}} \quad (2)$$

$$Z_b = \frac{\alpha Z_0}{\sqrt{1 - \alpha^2 |\sin \theta_b|}} \quad (3)$$

$$\tan \theta_a = -\frac{Z_b}{Z_a} \tan \theta_b \quad (4)$$

where  $Z_0$  is the port termination impedance.

With the help of (4), (2) and (3) can also be written in terms of  $\theta_a$  as follows:

$$Z_a = \frac{\alpha Z_0}{|\sin \theta_a|} \quad (5)$$

$$Z_b = \frac{\alpha Z_0}{\sqrt{\sin^2 \theta_a - \alpha^2}} \quad (6)$$

Advantage of this alternative representation shall be evident shortly.

## III. PROPOSED DUAL-BAND COUPLERS

The single-band BLC shown in Fig. 1 can be configured to work as a dual-band BLC by making appropriate changes in this structure. For this purpose, it is pertinent to consider sinusoid function that is present both in (2) as well as in (3). A half cycle of sinusoid is shown in Fig. 2. It is apparent that sinusoid remains the same at  $\theta$  and at  $\pi - \theta$ . Therefore, for example, if the vertical TLs are assigned electrical length  $\theta_b$  at  $f_1$  then its value should be selected in such a manner that when the frequency changes to  $f_2$ , the electrical length becomes  $\pi - \theta_b$ . This shall, ideally, guarantee the same performance at the two design frequencies. For a nondispersive TL, the electrical length ( $\theta$ ) is proportional to frequency ( $f$ ) [14],

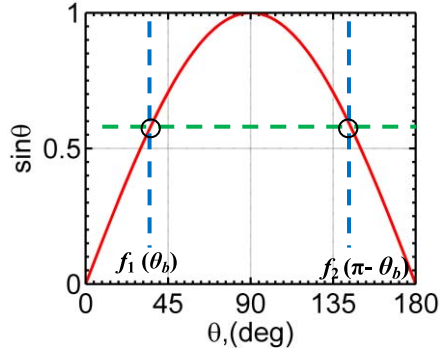


Fig. 2. Half cycle of a sinusoid. It has the same value at  $\theta$  and  $\pi - \theta$ .

and hence, one can write the following two equations for vertical TL sections:

$$\theta_b = kf_1 \quad (7)$$

$$\pi - \theta_b = kf_2 \quad (8)$$

where  $k$  is some constant with unit of radian per hertz.

The parameter  $\theta_b$  can be found by solving (7) and (8)

$$\theta_b = \pi / (1 + r) \quad (9)$$

where  $r = f_2/f_1$  is the band-ratio, and  $r > 1$ .

With  $\theta_b$  defined, the other parameter of the vertical TL sections, namely,  $Z_b$  can be determined using (3) for a given value of  $\alpha$ .

Unfortunately, the horizontal TL section for a dual-band BLC can no more be a simple TL shown in Fig. 1. It needs to be configured appropriately for dual-band operation. This statement can be mathematically justified as follows.

Since  $r > 1$ , it can be deduced from (9) that  $\theta_b < 90^\circ$ . Furthermore, the characteristic impedance is always positive and therefore  $Z_b/Z_a > 0$ . Combining these two facts it can be concluded that

$$\frac{Z_b}{Z_a} \tan \theta_b > 0. \quad (10)$$

Now, since (10) holds true, therefore from (4), the following expression can be deduced:

$$\theta_a = \pi - \tan^{-1} \left( \frac{Z_b}{Z_a} \tan \theta_b \right). \quad (11)$$

Noting that any  $\theta$  defined at  $f_1$  would become  $r\theta$  at  $f_2$ , since electrical length is proportional to frequency, evaluation of the left- and right-hand side of (4) at  $f_2$  results into the following expressions:

$$\begin{aligned} \text{L.H.S}|_{f_2} &= \tan \theta_a|_{f_2} = \tan r\theta_a \\ &= \tan \left( r\pi - r \tan^{-1} \left( \frac{Z_b}{Z_a} \tan \theta_b \right) \right) \end{aligned} \quad (12)$$

$$\text{R.H.S}|_{f_2} = - \left( \frac{Z_b}{Z_a} \tan \theta_b \right) |_{f_2} = - \frac{Z_b}{Z_a} \tan r\theta_b = \frac{Z_b}{Z_a} \tan \theta_b \quad (13)$$

where the fact  $r\theta_b = \pi - \theta_b$  has been used. Now, since L.H.S is a function of  $r$  whereas R.H.S is independent of  $r$ , therefore, in general, there does not exist a TL whose electrical length

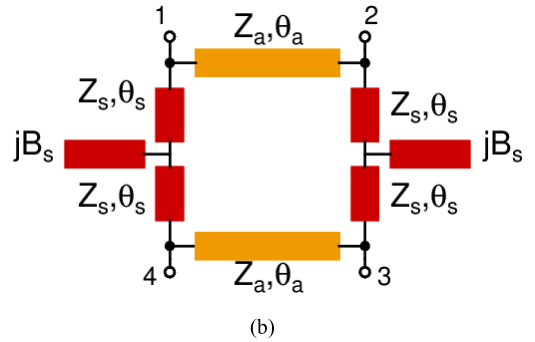
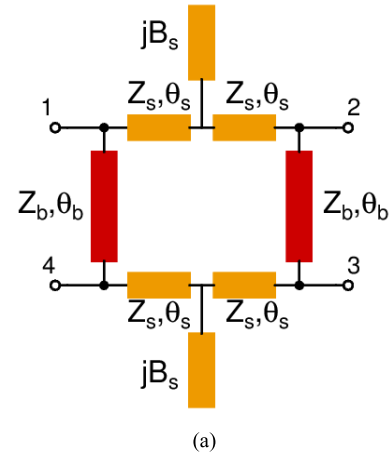


Fig. 3. Dual-band BLCs incorporating T-network. (a) Design A: vertical arm intact, horizontal arm replaced with a T-network. (b) Design B: horizontal arm intact, vertical arm replaced with a T-network.

can be found from (4) for dual-band application. This claim can also be supported logically as follows. At  $f_1$  (which is the lower frequency), it can be inferred from (4) that because of the presence of a negative sign in (4),  $\theta_a$  will be greater than  $90^\circ$  as  $\theta_b < 90^\circ$ . Therefore, at  $f_2$ ,  $\theta_a$  will need to be smaller than  $90^\circ$  considering that  $\theta_b > 90^\circ$ . Thus, it can be seen that when  $\theta_b$  is selected using (9), the resulting  $\theta_a$  must decrease with increase in frequency, an attribute not exhibited by a nondispersive TL. Thus, there is a need to synthesize a block which can satisfy (4). It has been widely reported that T- and Pi-networks provide this possibility.

#### A. Synthesis Using a T-Network

The modified BLC, called design A, is shown in Fig. 3(a), where the horizontal sections of Fig. 1 have been replaced by equivalent T-networks consisting of TL segments having characteristic impedance  $Z_s$  and electrical length  $\theta_s$  and the middle arm admittances of  $jB_s$ . Essentially, this T-network behaves as a line having characteristic impedance  $Z_a$  and electrical length  $\theta_a$  as regulated by (2)–(4) and (9).

By equating the ABCD parameter of the T-network to that of the original horizontal line, the following three equations are obtained:

$$\cos 2\theta_s - \frac{1}{2} B_s Z_s \sin 2\theta_s = \cos \theta_a \quad (14)$$

$$Z_s (\sin 2\theta_s - B_s Z_s \sin^2 \theta_s) = Z_a \sin \theta_a \quad (15)$$

$$\frac{1}{Z_s} (\sin 2\theta_s + B_s Z_s \cos^2 \theta_s) = \frac{\sin \theta_a}{Z_a}. \quad (16)$$

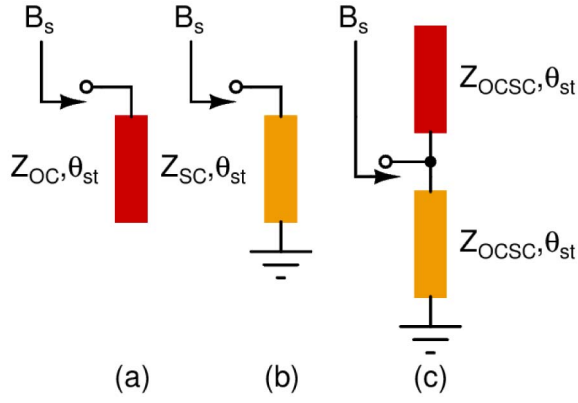


Fig. 4. Dual-band susceptance. (a) Open stub. (b) Short stub. (c) Combination of open–short stubs.

Moreover, the following two equations can be obtained from simplification of (14)–(16):

$$M = Z_s B_s = \frac{2[\cos 2\theta_s + \sqrt{1 - \alpha^2} |\cos \theta_b|]}{\sin 2\theta_s} \quad (17)$$

$$Z_s = Z_a \left( \frac{M + \sqrt{M^2 + 4 \sin^2 \theta_a}}{2 \sin \theta_a} \right). \quad (18)$$

Since  $Z_s$  is ideally constant with frequency, it is apparent from (17) that  $B_s$  just changes its sign as the frequency switches from  $f_1$  to  $f_2$ , if  $\theta_s = \theta_b$ . This type of admittance can be realized with a dual-band susceptance using a short-circuit or an open-circuit stub or a combination thereof, depicted in Fig. 4 [40], [41].

The design equations for these dual-band susceptances are summarized as follows:

$$Z_{SC} = -\frac{\cot \theta_{st}}{B_s} \quad (19)$$

$$Z_{OC} = \frac{\tan \theta_{st}}{B_s} \quad (20)$$

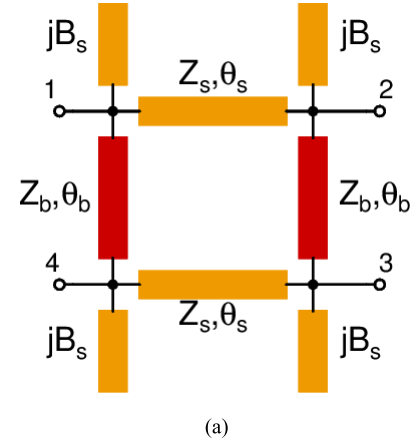
$$Z_{OCSC} = \frac{\tan^2 \theta_{st} - 1}{B_s \tan \theta_{st}} \quad (21)$$

where  $Z_{SC}$ ,  $Z_{OC}$ , and  $Z_{OCSC}$  are characteristic impedances of stubs in three cases. The electrical length of these stubs  $\theta_{st}$  is selected as integer multiple of  $\theta_s$  (usually equal to  $\theta_s$  or  $2\theta_s$ ) to get a positive value for the impedances of stubs and this depends on the sign of  $B_s$  [41].

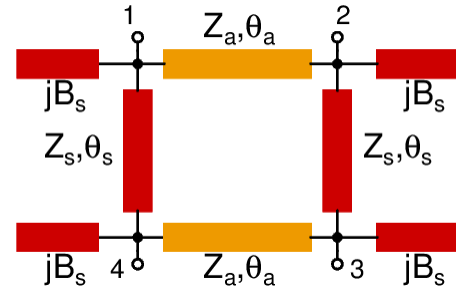
So far, the strategy was to let vertical line remain a normal TL and synthesize the horizontal ones with a T-network. A reverse process can also be used, that is, to let horizontal line remain a normal TL and synthesize the vertical ones with a T-network, as shown in Fig. 3(b). This structure is being called design B. Here comes the use of the alternative expression given in (5) and (6). It is apparent that in a manner similar to the previous case,  $\theta_a$  can now be selected as

$$\theta_a = \pi/(1 + r). \quad (22)$$

Repeating the above procedure of equating the ABCD matrix of a T-network, now with that of the vertical line,



(a)



(b)

Fig. 5. Dual-band BLCs incorporating Pi-network. (a) Design C: vertical arm intact, horizontal arm replaced with a Pi-network. (b) Design D: horizontal arm intact, vertical arm replaced with a Pi-network.

the following results ensue:

$$N = Z_s B_s = \frac{2[\cos 2\theta_s + |\cos \theta_a|/\sqrt{1 - \alpha^2}]}{\sin 2\theta_s} \quad (23)$$

$$Z_s = Z_b \left( \frac{N + \sqrt{N^2 + 4 \sin^2 \theta_b}}{2 \sin \theta_b} \right) \quad (24)$$

where  $\theta_s = \theta_a$  and, again, dual-band admittances can be realized with the help of (19)–(21).

### B. Synthesis Using a Pi-Network

The proposed design C is shown in Fig. 5(a). To obtain this configuration, each vertical line of the conventional BLC is replaced by Pi-network. A Pi-network consists of a transmission line segment having characteristics impedance  $Z_s$  and electrical length  $\theta_s$  and two side arms having admittances of  $jB_s$  each. The idea once again is to achieve dual-band functionality in terms of characteristic impedance and electrical length given by (2)–(4) and (9).

For the case shown in Fig. 5(a), equating the ABCD matrix of a Pi-network with that of the horizontal line of the BLC, the following two equations are obtained:

$$\cos \theta_s - B_s Z_s \sin \theta_s = \cos \theta_a \quad (25)$$

$$\frac{Z_s^2}{1 - B_s^2 Z_s^2 + 2B_s Z_s \cot \theta_s} = Z_a^2. \quad (26)$$

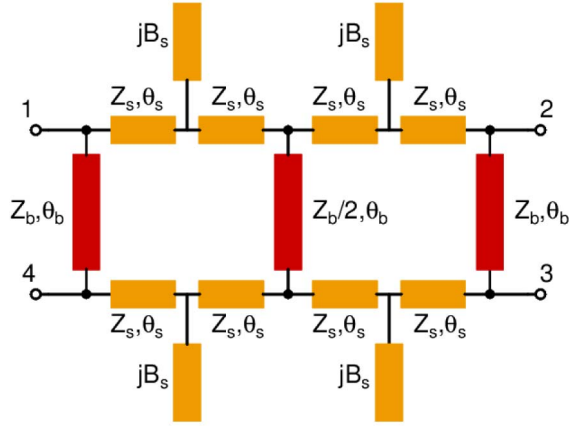


Fig. 6. Proposed dual-band crossover using the cascade of two dual-band BLCs of Fig. 3(a).

Solving (25) and (26), the following design equations are obtained:

$$Z_s = \sqrt{(1 - \alpha^2)} Z_b = \frac{\alpha Z_0}{|\sin \theta_b|} \quad (27)$$

$$B_s = \frac{1 + \sqrt{1 - \alpha^2}}{Z_s} \cot \theta_s = \left( \frac{1}{Z_s} + \frac{1}{Z_a} \right) \cot \theta_b \quad (28)$$

where  $\theta_s = \theta_b$ .

Similarly, for design D shown in Fig. 5(b), the following design equations can be obtained:

$$Z_s = Z_a / \sqrt{(1 - \alpha^2)} = \frac{\alpha Z_0}{\sqrt{(1 - \alpha^2)} |\sin \theta_a|} \quad (29)$$

$$B_s = \frac{1 + 1/\sqrt{1 - \alpha^2}}{Z_s} \cot \theta_s = \left( \frac{1}{Z_s} + \frac{1}{Z_a} \right) \cot \theta_a \quad (30)$$

where  $\theta_s = \theta_a$ .

A few important comments regarding the prospects of synthesis using a Pi-network are as follows.

- 1)  $B_s$  can again be realized using open or short stub with the design equations given by (19) and (20).
- 2) The combination of open–short stubs of Fig. 4(c) may not be useful in this case due to challenges in layout.
- 3) Interestingly,  $Z_s$  ( $Z_b$ ) of design C has the same expression as that of  $Z_a$  ( $Z_s$ ) of design D. Also, from (28) and (30), it is apparent that the final expression for  $B_s$  is the same for designs C and D. This point has a very important implication which will be apparent in the subsequent sections.

#### IV. DUAL-BAND CROSSOVER

It is well known that cascade of two BLCs can be used to construct a crossover [33]. This concept was used in [36] to design a dual-band crossover in which two dual-band BLCs like that shown in Fig. 5 were used. However, as shall be evident in the simulation section, the band-ratio is substantially larger if T-type BLCs (design A) are used. With this fact, the proposed crossover is shown in Fig. 6. The characteristic impedance of the common TL (seen in the middle) is halved and equals  $Z_b/2$ , as they are the parallel combination of TLs

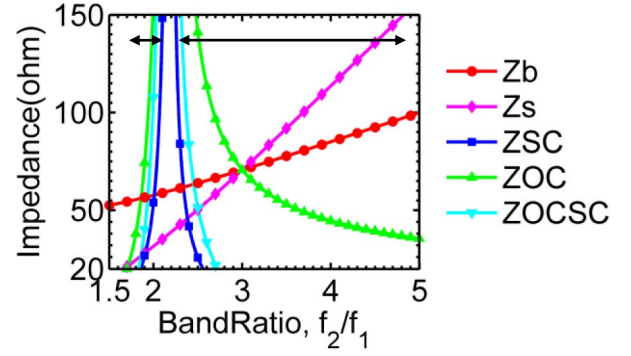


Fig. 7. Variation of characteristic impedances with band-ratio for design A.

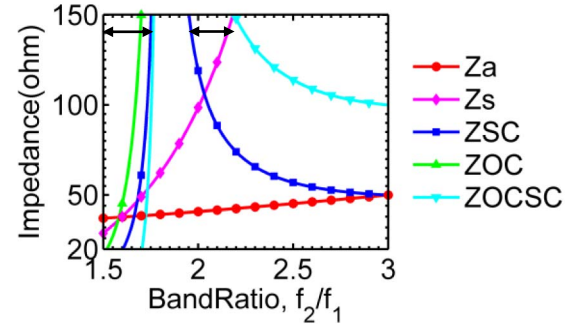


Fig. 8. Variation of characteristic impedances with band-ratio for design B.

having characteristic impedances of  $Z_b$ . It is also important to note at the outset that the T-type BLCs (design B) for crossover design should be avoided. The next section provides an elaborated discussion on this aspect.

#### V. SIMULATION AND DISCUSSION

In the first set of simulations, the T-network-based coupler with equal power division ( $\alpha^2 = 0.50$ ) is considered. Characteristic impedance is assumed to be limited within the range from 20 to 150  $\Omega$ . Fig. 7 shows the impedance variation for the TL sections of design A. The band-ratio range over which one can get realizable values of various TL sections is indicated by arrows. It is clear from Fig. 7 that with the choice of using open or short stubs or a combination thereof, on the higher side, the band-ratio ranges from 2.3 to 4.8. On the lower side, the band-ratio lies between 1.7 and 2.1. There is a gap, ranging from 2.1 to 2.3, where the required characteristic impedance for any type of the stubs is beyond 150  $\Omega$ .

At this moment, therefore, it is imperative to look at the other alternative, namely, design B, whose characteristic impedance variation is given in Fig. 8.

The value of  $Z_s$  shoots up rapidly in this case and the reason for such a behavior could be inferred from (2), (3), (5), and (6). Apparently, the denominator of neither (2) nor (3) equals zero for  $\theta_b < 90^\circ$  and  $0 < \alpha < 1$ . This situation is, however, different in the alternative form (6), where denominator of  $Z_b$  does move toward zero when  $\theta_a$  approaches toward  $45^\circ$  (i.e.,  $r = 3$ ), and hence, the stub characteristic impedance  $Z_s$  related to  $Z_b$  by (24) rises sharply. It can be identified from Fig. 8 that the band-ratio ranges from 1.5 to 1.75 and 1.95 to 2.2 in this case. Thus, with the choice of being able to

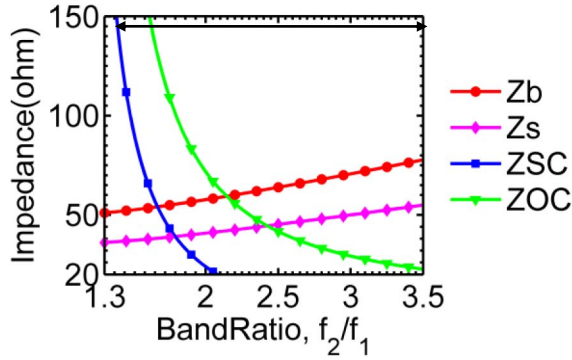


Fig. 9. Variation of characteristic impedances with band-ratio for design C.

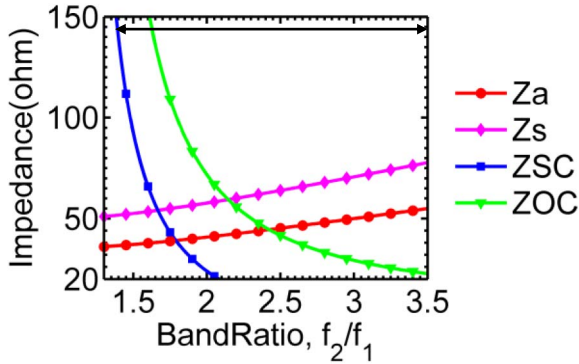


Fig. 10. Variation of characteristic impedances with band-ratio for design D.

use both the possible structures (i.e., designs A and B), this type of coupler can work seamlessly over the band-ratio range 1.5–4.8, with an exception of 2.2–2.3.

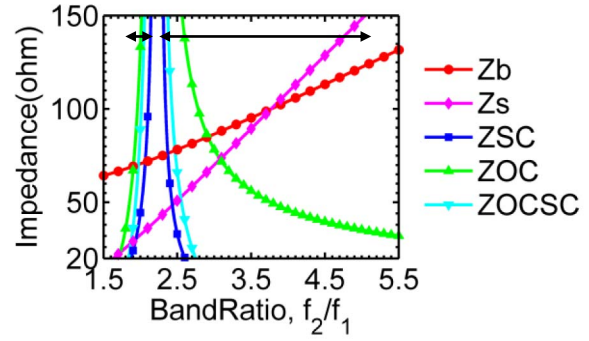
If the upper limit of impedance is assumed to be 120  $\Omega$  instead of 150  $\Omega$  [18], then the achievable band-ratio changes to slightly smaller values of 1.5–4.1, with a gap between 2.1 and 2.3. Compared with this, [18] has band-ratio of only 1.25–2.85 and apparently requires larger size as the integer  $m$  defined in [18] ranges from 1 to 6.

Similarly, Figs. 9 and 10 show the impedance variation for TL sections of Pi-network-based couplers of designs C and D, respectively ( $\alpha^2$  still equals 0.50). Comparing Figs. 9 and 10, it can be observed that as noticed during analysis,  $Z_s$  ( $Z_b$ ) in Fig. 9 has the same profile as that of  $Z_a$  ( $Z_s$ ) in Fig. 10.

Also,  $Z_{SC}/Z_{OC}$  are the same in both the cases as  $B_s$  remains the same for both the cases whether one synthesizes the horizontal or vertical lines of the BLC using a Pi-network. This is in stark contrast to the impedance profile exhibited by the TL section of the BLC realized using a T-network. Intuitively, this contrast can be attributed to the fact that the stubs in Fig. 5, whether produced by the vertical line or the horizontal Pi-networks, belong to the ports (corners), whereas the stubs in the case of the T-network of Fig. 3 belong to the arms.

It can also be seen in Figs. 9 and 10 that the band-ratio in this case ranges from 1.35 to 3.5 and it is similar to [16, Figs. 5 and 6].

In fact, the earlier reported design of a dual-band coupler [16] can be considered as a special case, with equal power division, i.e.,  $\alpha^2 = 0.50$ , of the design scheme reported


 Fig. 11. Variation of characteristic impedances with band-ratio for design A with  $\alpha^2 = 0.6$ .

in this paper. The reported work here is more generic and is capable of providing design strategy for unequal power division as well.

Furthermore, the term *fractional bandwidth*  $\delta$  defined in [16] can be expressed in terms of band-ratio  $r$  as  $\delta = (r - 1)/(r + 1)$ .

From the above discussion, it can be concluded that with the choice of synthesis using a T- or Pi-network, and short, open, or combined type of stubs, the overall band-ratio in the range 1.35–4.8 can be achieved. It can also be inferred from the above discussions that the use of a Pi-network (designs C and D) is appropriate for lower band-ratio synthesis while a T-network with the horizontal line replacement should be favored (design A) for relatively higher band-ratio synthesis.

Furthermore, a quick simulation reveals that the phase shift ( $90^\circ$ ) differs in sign at the two frequencies for design B, and this behavior is similar to the coupler reported in [26]. However, due to the rapid variation of  $Z_s$  for design B, this particular structure shall not be discussed further. Therefore, in subsequent discussions T-network based BLC refers to the configuration shown in Fig. 3(a), that is, design A. Similarly, since both the Pi-network BLCs of Fig. 5 are similar, only the BLC shown in Fig. 5(a) (design C) shall be discussed.

Now, the ability of the proposed structure for unequal power division ( $\alpha^2 > 0.5$ ) is explored. To that end, Figs. 11–13 show the impedance variations for  $\alpha^2 = 0.6, 0.7$ , and  $0.80$ , respectively, for design A. It can be observed in these plots that the T-network-based formulations for design of a dual-band coupler are indeed capable of unequal power division. However, it is also clear that the achievable band-ratio decreases with the increase in power division ratio. The reason can be deduced from (3), where  $\sqrt{1 - \alpha^2}$  decreases with increase in  $\alpha^2$ , since  $0 < \alpha^2 < 1$ , whereas  $\alpha$  increases with increase in  $\alpha^2$ .

The plots in Figs. 14–17 depict the impedance variation for design C, for  $\alpha^2 = 0.6, 0.7, 0.8$ , and  $0.85$ , respectively. Comparison of the results in Figs. 14–17 with those in Figs. 11–13 reveals that the available band-ratios in the case of Pi-network-based BLCs (design C) are continuous, ranging from 1.35 to 3.3 for  $\alpha^2 = 0.80$ . Finally, it is evident from Figs. 14–17 that the band-ratio decreases even for design C with the increase in  $\alpha^2$ .

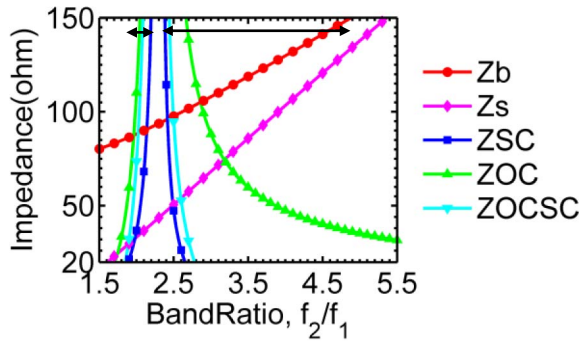


Fig. 12. Variation of characteristic impedances with band-ratio for design A with  $\alpha^2 = 0.7$ .

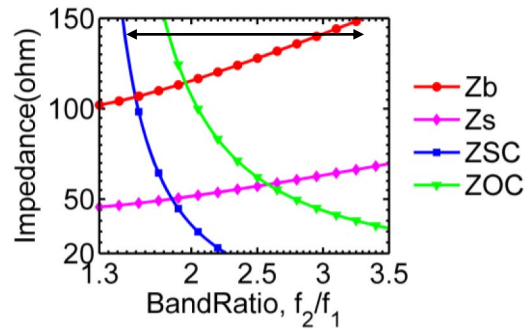


Fig. 16. Variation of characteristic impedances with band-ratio for design C with  $\alpha^2 = 0.80$ .

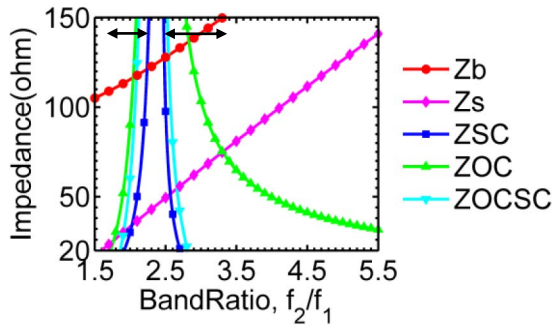


Fig. 13. Variation of characteristic impedances with band-ratio for design A with  $\alpha^2 = 0.8$ .

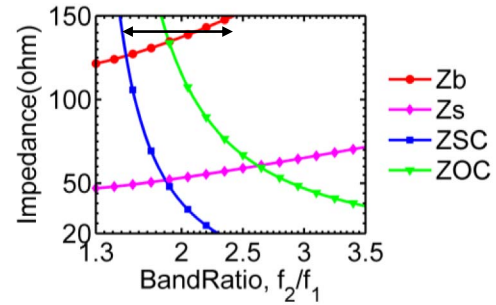


Fig. 17. Variation of characteristic impedances with band-ratio for design C with  $\alpha^2 = 0.85$ .

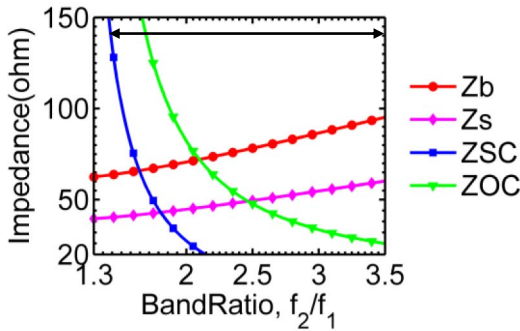


Fig. 14. Variation of characteristic impedances with band-ratio for design C with  $\alpha^2 = 0.60$ .

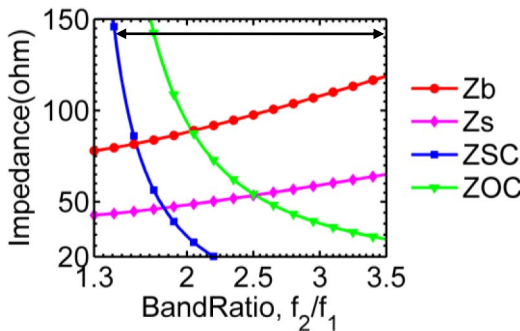


Fig. 15. Variation of characteristic impedances with band-ratio for design C with  $\alpha^2 = 0.70$ .

It is important to note that the junction discontinuities, end effects in the open stubs, and via in the short stubs will cause departure from the ideal behavior of the proposed designs. And, therefore, tuning/optimization may be required during the

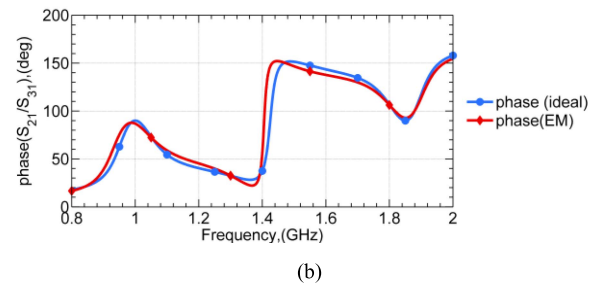
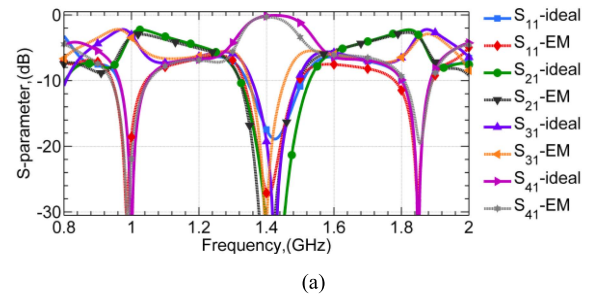


Fig. 18. Ideal and EM simulated performance of a 3-dB BLC (design A). (a) S-parameters. (b) Phase difference.

final implementation. As an example, Fig. 18 depicts the ideal and optimized electromagnetic (EM) simulation performance of a 3-dB coupler, design A, for  $r = 1.85$ . For this design:  $Z_b = 56.04 \Omega$ ,  $Z_s = 26.28 \Omega$ , and  $\theta_b = \theta_s = 63.16^\circ$ . The middle arm admittances are realized using open-short combination stubs having  $Z_{OCSC} = 24.27 \Omega$  and  $\theta_{st} = 126.32^\circ$ . As the values of impedances are low, an alumina substrate with  $\epsilon_r = 9.9$  and  $35 \mu\text{m}$  copper is assumed for EM simulation.

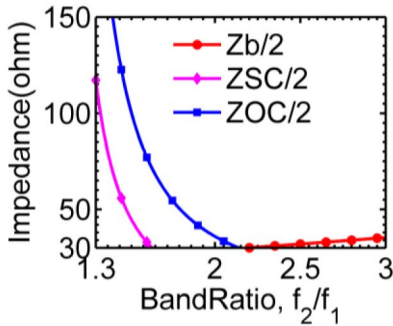


Fig. 19. Variation of halves of the characteristic impedances assuming the minimum realizable impedance to be  $30 \Omega$ , with Pi-network.

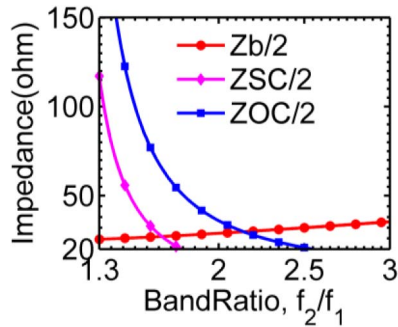


Fig. 20. Variation of halves of the characteristic impedances assuming the minimum realizable impedance to be  $20 \Omega$ , with Pi-network.

In this case, the EM simulated transmissions  $S_{21}/S_{31}$  are  $-3.28/-3.2$  dB at  $f_1$  and  $-3.43/-3.37$  dB at  $f_2$ .

Next, to investigate the performance of the proposed T-network dual-band crossover, initially the Pi-network-based crossover presented in [36] is considered. As mentioned earlier, the crossover shown in [36, Fig. 2] is cascade connection of two BLCs shown here in Fig. 5. Therefore, the plots in Figs. 9 and 10 along with the results shown in Fig. 19, where halves of characteristic impedances are plotted, are considered for comprehending the reported crossover in [36]. Subsequently, the following two inferences can be drawn for Pi-type crossover reported in [36].

- 1) The highest range of band-ratio deduced in [36] is 2.96. However, this is misleading as [36, Fig. 7] does not consider halves of characteristic impedances. Considering  $30 \Omega$  to be the minimum realizable impedance as assumed in [36], crossovers cannot even be realized, at all, since according to Fig. 19,  $Z_b/2$  begins to increase above  $30 \Omega$  when the stubs are not realizable. In contrast, for the minimum allowable impedance of  $20 \Omega$ , the maximum band-ratio is around 2.5 as shown in Fig. 20.
- 2) The minimum band-ratio in [36] was limited to 1.71 due to the adopted design strategy. For realization of crossover with smaller band-ratio, the Pi-network-based dual-band coupler design strategy, utilizing short stubs, proposed in this paper can be used. It is evident from Figs. 9 and 20 that the minimum band-ratio could be 1.35 in such a situation.

The capability of the proposed dual-band crossover shown in Fig. 6 can be studied from Figs. 7 and 21. It is clear that

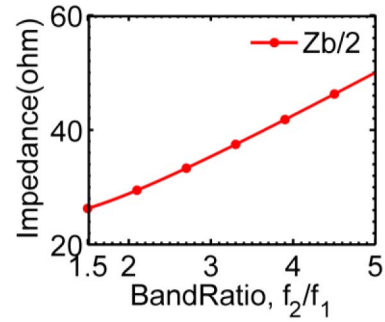


Fig. 21. Variation of halves of the characteristic impedances assuming the minimum realizable impedance to be  $20 \Omega$ , with T-network.

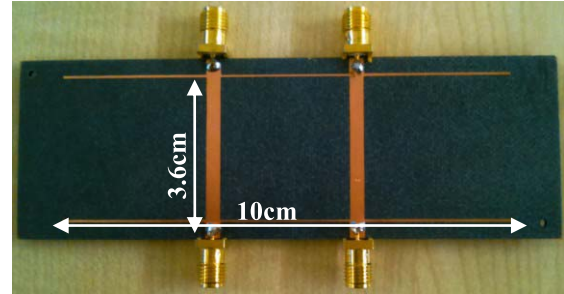


Fig. 22. Fabricated BLC design C prototype with  $\alpha^2 = 0.60$ .

the impedance  $Z_b/2$  of the middle arm of the crossover can still be realized. Apparently the band-ratio of the crossover also ranges from 2.3 to 4.8 on the higher side. Therefore, it would a good strategy to use the modified crossover, with Pi-structure discussed above, for smaller band-ratios and the proposed crossover with T-structure for the larger band-ratios. Combined together, these two designs offer simple layout with a band-ratio ranging from 1.35 to 4.8, the highest reported in the literature.

## VI. PROTOTYPES AND MEASUREMENT

To experimentally verify the presented concepts, two prototypes are fabricated on RT/Duroid 5880 (substrate  $\epsilon_r = 2.2$ , substrate thickness = 1.575 mm, and copper cladding =  $35 \mu\text{m}$ ).

The first prototype, depicted in Fig. 22, is the Pi-network-based dual-band BLC [Fig. 5(a), design C] with  $\alpha^2 = 0.6$  (i.e., for unequal power division). The two design frequencies are assumed to be  $f_1 = 1$  GHz and  $f_2 = 2$  GHz. Using the formulas discussed previously, the design values come out to be  $Z_b = 115.47 \Omega$ ,  $Z_S = 51.64 \Omega$ , and  $\theta_b = \theta_s = 60^\circ$ . The side arm admittances are realized using open stubs with  $Z_{OC} = 107.05 \Omega$  and  $\theta_{st} = 60^\circ$ . The corresponding EM simulation results and the measured results are compared in Fig. 23. Isolation and return loss are better than  $-30$  dB, whereas transmission  $S_{31}$  is  $-7.4$  and  $-7$  dB and they are slightly off from the ideal value of  $-6.9$  dB. This structure was optimized for correct differential phase of ( $S_{21}-S_{31}$ ) as this is important in realization of crossover by cascading technique. The measured differential phase is  $90.2^\circ$  and  $90.3^\circ$  at the two frequencies and could be categorized as extremely well behaved.

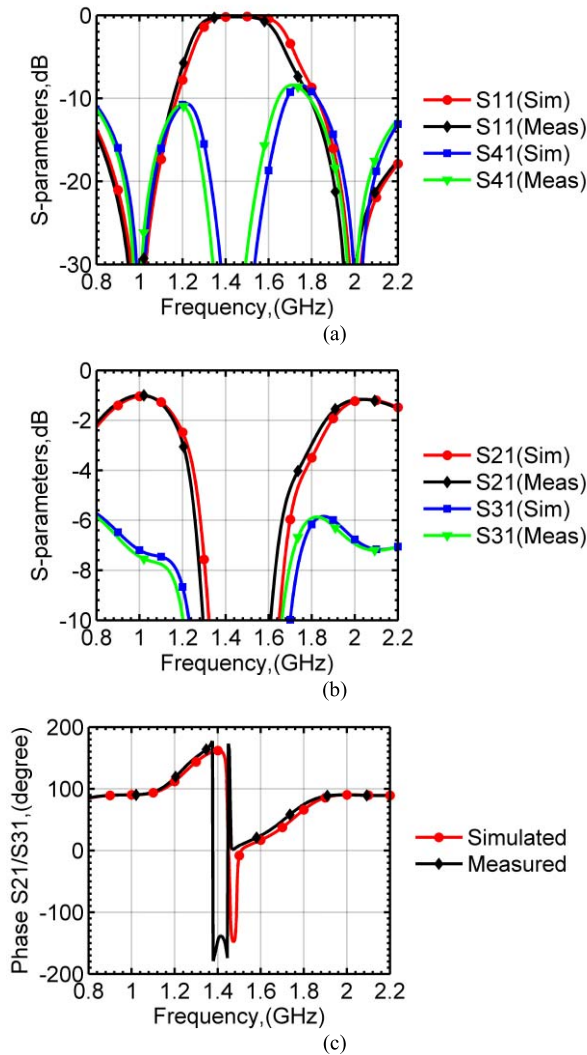


Fig. 23. Simulated and measured results of the fabricated BLC. (a) Matching and isolation parameters. (b) Transmission parameters. (c) Phase difference.

The second prototype, depicted in Fig. 24, is the T-network-based dual-band crossover discussed in Section IV. For the first time, a dual-band crossover with such a simple layout is being reported. The two chosen design frequencies are  $f_1 = 1$  GHz and  $f_2 = 4$  GHz. Once again, using the formulas discussed previously, the calculated design values are  $Z_b = 85.06 \Omega$ ,  $Z_s = 113.71 \Omega$ , and  $\theta_b = \theta_s = 36^\circ$ . The side arm admittances are realized using open stubs with  $Z_{oc} = 44.59 \Omega$  and  $\theta_{st} = 36^\circ$ .

It is important to consider two points for this design. First, although the electrical length of lines having characteristic impedance of  $Z_b$  and  $Z_b/2$  are the same, their physical dimensions will differ from each other slightly considering that they are functions of electrical length as well as the characteristic impedance. Thus, to make the layout simpler, the final device was optimized to make their lengths equal. Second, usually the four stubs should be folded to set the same into the inside vacant spaces of the crossover, but in this particular example, the conductors were thick so it was not attempted. The simulated and measured results for the crossover are shown in Fig. 25. It is apparent that S11, S41, and S21

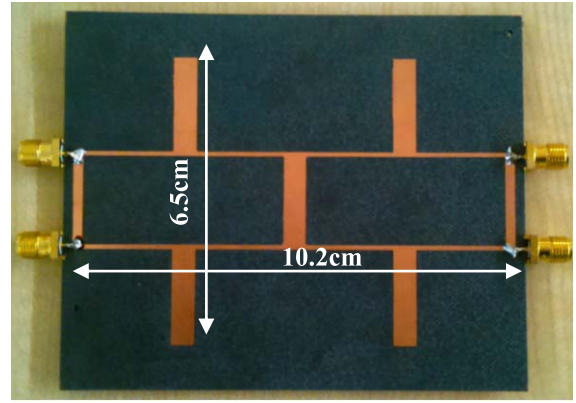


Fig. 24. Fabricated dual-band crossover prototype.

are better than  $-15$  dB. The transmission S31, which should ideally be equal to 0 dB, is  $-0.4$  and  $-1.1$  dB in this case. However, these are around the acceptable limits of  $-1$  dB reported earlier [35]. In addition, the relatively higher deviation in the proposed design could also be attributed to the fact that (9) and (22) were derived assuming the electrical length to be proportional to frequency (all the dual-band designs reported in the literature whose solutions are similar are based on this assumption as well). However, in practice, it is not the case as the effective dielectric constant itself is frequency dependent [42]. The phase  $\angle S31$  is found to be  $87^\circ$  and  $89^\circ$  at two frequencies as shown in Fig. 25(c). It is also to be noted that like the existing literature [34]–[38], the proposed design also does not incorporate  $50 \Omega$  connecting lines at all four ports. The reason is that, unlike a coupler where differential phase is important, in crossover absolute  $\angle S31$  is important. Thus, adding any length to the port in case of crossover would cause  $\angle S31$  to be different from the ideal value of  $90^\circ$ .

It is also interesting to note that the characteristic of the proposed dual-band crossover is narrow band, much like that reported in [35]. Just to compare, a crossover is designed using the proposed method for  $r = 1.9$ , with the design parameters as  $Z_b = 56.59 \Omega$ ,  $Z_s = 28.03 \Omega$ , and  $\theta_b = \theta_s = 62.07^\circ$ . The side arm admittances are realized using short stubs with  $Z_{sc} = 26.74 \Omega$  and  $\theta_{st} = 62.07^\circ$ . The simulated result is shown in Fig. 26. A comparison of this result with the result shown in [35, Fig. 6(a)] reveals that the bandwidth of the crossover is comparable and better than the one reported in [35]. This observation is also true for the proposed dual-band couplers. In fact, this also confirms the observation made in [39] that BLCs based on unequal branch length are inherently narrow band in nature.

Comparison of the proposed dual-band crossover scheme with some recently reported works on dual-band crossover is given in Table I. Layout complexity is an important parameter for crossover as usually these are larger in size than BLCs. Higher complexity in the layout is marked with more number of asterisks in Table I. It is emphasized that the achievable band-ratio of the proposed scheme is the highest among the reported designs when layout simplicity is considered. Furthermore, the length of various arms in the different crossover structures reported in the state-of-the-art is given by the same formula as (9)/(22), and hence, a convenient way

TABLE I  
 COMPARISON OF DUAL-BAND CROSSOVER WITH CURRENT STATE-OF-THE-ART

References	TMTT [34]	TMTT [35]	E. Lett. [36]	TMTT [37]	MWCL[38]	This Work
Year	2011	2012	2012	2013	2015	2016
Configuration	Three section BLC	Window-shaped structure (T)	Two section BLC	Two section BLC	Window-shaped structure ( $\pi$ )	Two section BLC
Band-ratio	NA- 2.25	1.6-4	1.71-2.96	1.5-2	2-7	1.35-4.8
Size	$3\theta_b \times 1\theta_b$	$4\theta_b \times 4\theta_b$	$2\theta_b \times 3\theta_b$	$2\theta_b \times 2\theta_b$	$4\theta_b \times 4\theta_b$	$4\theta_b \times 1\theta_b$ (T-type); $2\theta_b \times 3\theta_b$ (Pi-type)
Layout Complexity	*	**	*	*	****	*

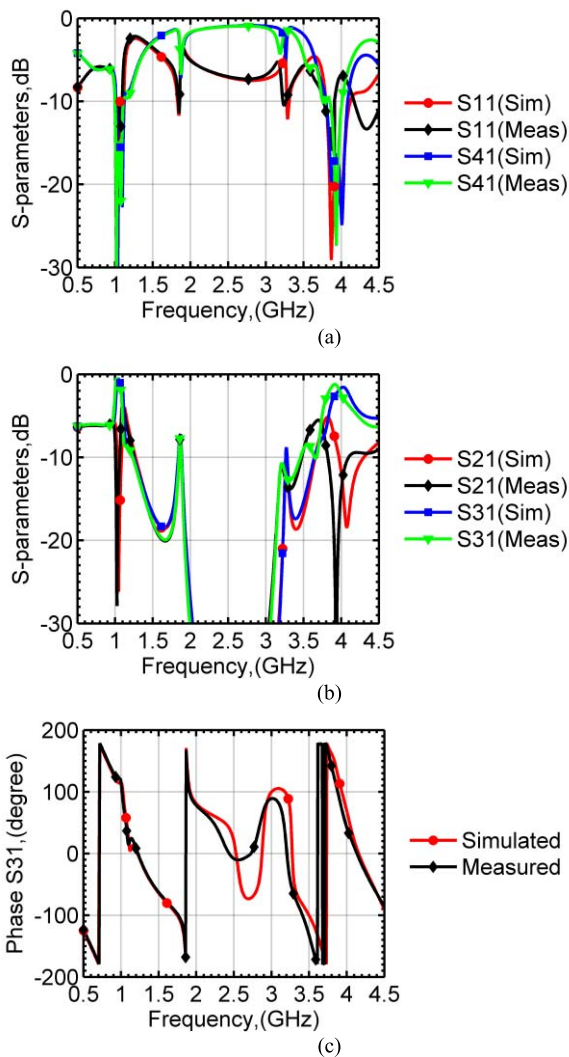


Fig. 25. Simulated and measured results of the fabricated crossover. (a) Matching and isolation parameters. (b) Transmission parameters. (c) Phase.

to compare different designs is in terms of  $\theta_b$ . There are two possible sizes in the proposed crossover scheme as there are two possible cases, namely, Pi-type and T-type. Also, the size mentioned for the proposed crossover with a T-type BLC is based on the assumption that normally the stubs could fit inside the vacant spaces.

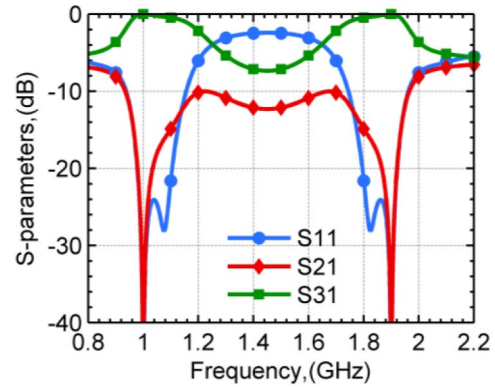


Fig. 26. Simulation results of the proposed crossovers example at 1/1.9 GHz.

## VII. CONCLUSION

A single-band unequal branch length coupler was investigated and a generalized formulation for the design of its dual-band version was obtained. Furthermore, it was shown that four different configurations of a dual-band coupler result from such a formulation. Each of these configurations was analyzed to assess their capability in terms of power division ratio and band-ratio. It is concluded that by having option of realizing any of these configurations, a wide range of power division and band-ratio could be obtained. Moreover, for the first time, technique to design a very wide frequency ratio crossover having simpler board layout was implemented to show the viability of the proposed techniques. A challenge in the dual-band design for a wide frequency ratio crossover was also identified, namely, the variation of effective dielectric constant with frequency, which causes the performance at the two frequencies to deviate from the ideal. An inherent limitation of the proposed technique is narrow bandwidth owing to the use of unequal branch lengths.

## REFERENCES

- [1] M. Zhou, J. Shao, B. Arigong, H. Ren, R. Zhou, and H. Zhang, "A varactor based 90° directional coupler with tunable coupling ratios and reconfigurable responses," *IEEE Trans. Microw. Theory Techn.*, vol. 62, no. 3, pp. 416–421, Mar. 2014.
- [2] J. L. Li and B. Z. Wang, "Novel design of Wilkinson power dividers with arbitrary power division ratios," *IEEE Trans. Ind. Electron.*, vol. 58, no. 6, pp. 2541–2546, Jun. 2011.
- [3] T.-S. Horng, "A rigorous study of microstrip crossovers and their possible improvements," *IEEE Trans. Microw. Theory Techn.*, vol. 42, no. 9, pp. 1802–1806, Sep. 1994.

- [4] H. Hashemi and A. Hajimiri, "Concurrent multiband low-noise amplifiers-theory, design, and applications," *IEEE Trans. Microw. Theory Technol.*, vol. 50, no. 1, pp. 288–301, Jan. 2002.
- [5] L.-S. Wu, J. Mao, and W.-Y. Yin, "Miniaturization of rat-race coupler with dual-band arbitrary power divisions based on stepped-impedance double-sided parallel-strip line," *IEEE Trans. Compon., Packag., Manuf. Technol.*, vol. 2, no. 12, pp. 2017–2030, Dec. 2012.
- [6] A. Genc, A. Baktur, and R. J. Jost, "Dual-bandpass filters with individually controllable passbands," *IEEE Trans. Compon., Packag., Manuf. Technol.*, vol. 3, no. 1, pp. 105–112, Jan. 2013.
- [7] Y. Liu, W. Chen, X. Li, and Z. Feng, "Design of compact dual-band power dividers with frequency-dependent division ratios based on multisection coupled line," *IEEE Trans. Compon., Packag., Manuf. Technol.*, vol. 3, no. 3, pp. 467–475, Mar. 2013.
- [8] P.-L. Chi and C.-C. Liu, "Novel dual-band quasi-0-dB coupled-line coupler using the composite right/left-handed transmission lines," *IEEE Trans. Compon., Packag., Manuf. Technol.*, vol. 4, no. 2, pp. 259–267, Feb. 2014.
- [9] S. Y. Zheng, Y. Wu, Y. Li, Y. Liu, and Y. Long, "Dual-band hybrid coupler with arbitrary power division ratios over the two bands," *IEEE Trans. Compon., Packag., Manuf. Technol.*, vol. 4, no. 8, pp. 1347–1358, Aug. 2014.
- [10] H. L. Zhang, B. J. Hu, and X. Y. Zhang, "Compact equal and unequal dual-frequency power dividers based on composite right/left-handed transmission lines," *IEEE Trans. Ind. Electron.*, vol. 59, no. 9, pp. 3464–3472, Sep. 2012.
- [11] X. Y. Zhang, C. H. Chan, Q. Xue, and B. J. Hu, "RF tunable bandstop filters with constant bandwidth based on a doublet configuration," *IEEE Trans. Ind. Electron.*, vol. 59, no. 2, pp. 1257–1265, Feb. 2012.
- [12] M. Bemani and S. Nikmehr, "Nonradiating arbitrary dual-band equal and unequal 1:4 series power dividers based on CRLH-TL structures," *IEEE Trans. Ind. Electron.*, vol. 61, no. 3, pp. 1223–1234, Mar. 2014.
- [13] Y. Wu, S. Y. Zheng, S. W. Leung, Y. Liu, and Q. Xue, "An analytical design method for a novel dual-band unequal coupler with four arbitrary terminated resistances," *IEEE Trans. Ind. Electron.*, vol. 61, no. 10, pp. 5509–5516, Oct. 2014.
- [14] K. Rawat, M. S. Hashmi, and F. M. Ghannouchi, "Dual-band RF circuits and components for multi-standard software defined radios," *IEEE Circuits Syst. Mag.*, vol. 12, no. 1, pp. 12–32, Feb. 2012.
- [15] I.-H. Lin, M. DeVincentis, C. Caloz, and T. Itoh, "Arbitrary dual-band components using composite right/left-handed transmission lines," *IEEE Trans. Microw. Theory Technol.*, vol. 52, no. 4, pp. 1142–1149, Apr. 2004.
- [16] K.-K. M. Cheng and F.-L. Wong, "A novel approach to the design and implementation of dual-band compact planar 90° branch-line coupler," *IEEE Trans. Microw. Theory Technol.*, vol. 52, no. 11, pp. 2458–2463, Nov. 2004.
- [17] K.-K. M. Cheng and S. Yeung, "A novel dual-band 3-dB branch-line coupler design with controllable bandwidths," *IEEE Trans. Microw. Theory Technol.*, vol. 60, no. 10, pp. 3055–3061, Oct. 2012.
- [18] H. Zhang and K. J. Chen, "A stub tapped branch-line coupler for dual-band operations," *IEEE Microw. Wireless Compon. Lett.*, vol. 17, no. 2, pp. 106–108, Feb. 2007.
- [19] H. Ren, J. Shao, M. Zhou, B. Arigong, J. Ding, and H. Zhang, "Design of dual-band transmission line with flexible phase shifts and its applications," *IET Electron. Lett.*, vol. 51, no. 3, pp. 261–262, Feb. 2015.
- [20] K.-S. Chin, K.-M. Lin, Y.-H. Wei, T.-H. Tseng, and Y.-J. Yang, "Compact dual-band branch-line and rat-race couplers with stepped-impedance-stub lines," *IEEE Trans. Microw. Theory Technol.*, vol. 58, no. 5, pp. 1213–1221, May 2010.
- [21] C.-L. Hsu, J.-T. Kuo, and C.-W. Chang, "Miniaturized dual-band hybrid couplers with arbitrary power division ratios," *IEEE Trans. Microw. Theory Technol.*, vol. 57, no. 1, pp. 149–156, Jan. 2009.
- [22] E. E. Djoumessi, E. Marsan, C. Caloz, M. Chaker, and K. Wu, "Varactor-tuned dual-band quadrature hybrid coupler," *IEEE Microw. Wireless Compon. Lett.*, vol. 16, no. 11, pp. 603–605, Nov. 2006.
- [23] Q. Liu *et al.*, "Generalized impedance-transforming dual-band branch-line couplers for arbitrary coupling levels," *Prog. Electromagn. Res. B*, vol. 53, pp. 399–415, 2013, doi: 10.2528/PIERB13061717.
- [24] P.-L. Chi and K.-L. Ho, "Design of dual-band coupler with arbitrary power division ratios and phase differences," *IEEE Trans. Microw. Theory Technol.*, vol. 62, no. 12, pp. 2965–2974, Dec. 2014.
- [25] L. K. Yeung, "A compact dual-band 90° coupler with coupled-line sections," *IEEE Trans. Microw. Theory Technol.*, vol. 59, no. 9, pp. 2227–2232, Sep. 2011.
- [26] C.-H. Yu and Y.-H. Pang, "Dual-band unequal-power quadrature branch-line coupler with coupled lines," *IEEE Microw. Wireless Compon. Lett.*, vol. 23, no. 1, pp. 10–12, Jan. 2013.
- [27] X. Wang, W.-Y. Yin, and K.-L. Wu, "A dual-band coupled-line coupler with an arbitrary coupling coefficient," *IEEE Trans. Microw. Theory Technol.*, vol. 60, no. 4, pp. 945–951, Apr. 2012.
- [28] M.-J. Park and B. Lee, "Dual-band, cross coupled branch line coupler," *IEEE Microw. Wireless Compon. Lett.*, vol. 15, no. 10, pp. 655–657, Oct. 2005.
- [29] H. Kim, B. Lee, and M.-J. Park, "Dual-band branch-line coupler with port extensions," *IEEE Trans. Microw. Theory Technol.*, vol. 58, no. 3, pp. 651–655, Mar. 2010.
- [30] Y. S. Wong, S. Y. Zheng, and W. S. Chan, "Multifolded bandwidth branch line coupler with filtering characteristic using coupled port feeding," *Prog. Electromagn. Res.*, vol. 118, pp. 17–35, 2011, doi: 10.2528/PIER11041401.
- [31] G. P. Riblet, "A directional coupler with very flat coupling," *IEEE Trans. Microw. Theory Technol.*, vol. 26, no. 2, pp. 70–74, Feb. 1978.
- [32] M.-J. Park, "Dual-band, unequal length branch-line coupler with center-tapped stubs," *IEEE Microw. Wireless Compon. Lett.*, vol. 19, no. 10, pp. 617–619, Oct. 2009.
- [33] J. S. Wight, W. J. Chudobiak, and V. Makios, "A microstrip and stripline crossover structure," *IEEE Trans. Microw. Theory Technol.*, vol. 24, no. 5, p. 270, May 1976.
- [34] F.-L. Wong and K.-K. M. Cheng, "A novel, planar, and compact crossover design for dual-band applications," *IEEE Trans. Microw. Theory Technol.*, vol. 59, no. 3, pp. 568–573, Mar. 2011.
- [35] J. Shao, H. Ren, B. Arigong, C. Li, and H. Zhang, "A fully symmetrical crossover and its dual-frequency application," *IEEE Trans. Microw. Theory Technol.*, vol. 60, no. 8, pp. 2410–2416, Aug. 2012.
- [36] Z.-W. Lee and Y.-H. Pang, "Compact planar dual-band crossover using two-section branch-line coupler," *IET Electron. Lett.*, vol. 48, no. 21, pp. 1348–1349, Oct. 2012.
- [37] F. Lin, Q.-X. Chu, and S. W. Wong, "Dual-band planar crossover with two-section branch-line structure," *IEEE Trans. Microw. Theory Technol.*, vol. 61, no. 6, pp. 2309–2316, Jun. 2013.
- [38] C.-W. Tang, K.-C. Lin, and W.-M. Chuang, "Design of a microstrip dual-band crossover with asymmetrical  $\pi$ -shaped transmission lines," *IEEE Microw. Wireless Compon. Lett.*, vol. 25, no. 9, pp. 588–590, Sep. 2015.
- [39] C. Toker, M. Saglam, M. Ozme, and N. Gunalp, "Branch-line couplers using unequal line lengths," *IEEE Trans. Microw. Theory Technol.*, vol. 49, no. 4, pp. 718–721, Apr. 2001.
- [40] M. A. Maktoomi, M. S. Hashmi, and F. M. Ghannouchi, "A T-section dual-band matching network for frequency-dependent complex loads incorporating coupled line with DC-block property suitable for dual-band transistor amplifiers," *Prog. Electromagn. Res. C*, vol. 54, pp. 75–84, 2014, doi: 10.2528/PIERC14090403.
- [41] M. A. Maktoomi and M. S. Hashmi, "A coupled-line based L-section DC-isolated dual-band real to real impedance transformer and its application to a dual-band T-junction power divider," *Prog. Electromagn. Res. C*, vol. 55, pp. 95–104, 2014, doi: 10.2528/PIERC14110502.
- [42] R. Garg, I. Bahl, and M. Bozzi, *Microstrip Lines and Slotlines*, 3rd ed. Norwood, MA, USA: Artech House, 2013.



**Mohammad A. Maktoomi** (GSM'14) received the B.Tech. degree in electronics engineering from Aligarh Muslim University (AMU), Aligarh, India, in 2009. He is currently pursuing the Ph.D. degree with the Electronics and Communication Engineering Department (RF/Microwave), Indraprastha Institute of Information Technology Delhi, New Delhi, India.

He has served with the Hindustan College of Science and Technology, Mathura, India, as an Assistant Professor, and AMU as a Guest Faculty Member. He is currently with the iRadio Laboratory, University of Calgary, Calgary, AB, Canada, as a Visiting Ph.D. Student. He has published in many international conferences and reputed journals. His current research interests include multiband RF/microwave circuits and current-mode analog circuits.

Mr. Maktoomi was a recipient of the Best Student Paper Award at the IEEE IMPACT, India, in 2013, in the RF/microwave category. He has been a Reviewer for many international conferences and journals and has been invited to many workshops to present tutorials.



**Mohammad S. Hashmi** (S'04–M'09) received the B.Tech. degree from Aligarh Muslim University, Aligarh, India, the M.S. degree from the Darmstadt University of Technology, Darmstadt, Germany, and the Ph.D. degree from Cardiff University, Cardiff, U.K.

He held research and engineering positions with the University of Calgary, Calgary, AB, Canada, Cardiff University, Thales Electronics GmbH, Ditzingen, Germany, and the Philips Technology Center, Aachen, Germany. He is currently an Assis-

tant Professor with the Indraprastha Institute of Information Technology Delhi, New Delhi, India. His research activities have led to one book, three patents (one pending), and over 75 publications. His current research interests include advanced RF circuits and systems, broadband linear and efficient power amplifiers for mobile and satellite applications, and high and low frequency instrumentation.

Dr. Hashmi recently joined as an Acquisition Editor of the Editorial Board of the *IEEE Microwave Magazine*.



**Fadhel M. Ghannouchi** (F'07) is currently a Professor and the iCORE/Canada Research Chair with the Department of Electrical and Computer Engineering, Schulich School of Engineering, University of Calgary, Calgary, AB, Canada, and the Director of the Intelligent RF Radio Laboratory. He has held numerous invited positions with several academic and research institutions in Europe, North America, and Japan. He has provided consulting services to a number of microwave and wireless communications companies. He has authored or co-authored over 650 publications. He holds ten U.S. patents with five pending. His current research interests include microwave instrumentation and measurements, nonlinear modeling of microwave devices and communications systems, design of power and spectrum efficient microwave amplification systems, and design of intelligent RF transceivers for wireless and satellite communications.